

Ultrafast behavior of the polarization filtering in anisotropically strained M -plane GaN films: A time-resolved pump-probe spectroscopy study

T. Flissikowski,* K. Omae,† P. Misra, O. Brandt, and H. T. Grahn

Paul-Drude-Institut für Festkörperelektronik, Hausvogteiplatz 5-7, 10117 Berlin, Germany

(Received 21 February 2006; revised manuscript received 9 May 2006; published 29 August 2006)

The dynamic behavior of the polarization filtering in M -plane GaN films is studied by time-resolved pump-and-probe spectroscopy. The reduced in-plane crystal symmetry and the anisotropic in-plane strain in M -plane GaN films lead to different absorption coefficients along the two principle in-plane axes. The absorption can be selectively bleached by additional pumping with polarized light along one of these two axes. On an ultrafast time scale, the resulting pump-and-probe transients are governed by two different processes, namely the relaxation dynamics of holes in the two uppermost valence bands and the coherent coupling artifact. Polarization-resolved pump-and-probe experiments at room temperature and below are performed in order to determine which of these two processes has the strongest influence on the transients. Furthermore, the recovery of the absorption is analyzed using the time symmetry of the coherent coupling artifact and a rate-equation model for carrier relaxation and redistribution in the valence bands. The analysis yields redistribution times below 1 ps and carrier recombination times of about 15 ps. Furthermore, the redistribution always leads to a comparable occupation of both valence bands, even if only one band is directly pumped.

DOI: [10.1103/PhysRevB.74.085323](https://doi.org/10.1103/PhysRevB.74.085323)

PACS number(s): 78.47.+p, 78.66.Fd, 42.25.Ja

I. INTRODUCTION

Optical modulators that have both a fast response and a high contrast can be realized on the basis of semiconductors that exhibit an optical polarization anisotropy.^{1,2} It has been previously demonstrated that strained M -plane GaN films, where the unique c axis lies in the film plane, exhibit a very large in-plane polarization anisotropy.³ In particular for a certain range of in-plane strain values, the wave function of the highest (second highest) valence band (VB) becomes completely $|x\rangle$ -like ($|z\rangle$ -like), which leads to an enhanced absorption coefficient α_{\perp} for the electric field component perpendicular to the c axis ($\mathbf{E} \perp \mathbf{c}$) compared to α_{\parallel} for the electric field component parallel to the c axis ($\mathbf{E} \parallel \mathbf{c}$). As a result, the component $\mathbf{E} \perp \mathbf{c}$ of a linearly polarized incident light beam is filtered after transmission through the film, appearing in the experiment as a rotation of the polarization vector toward the c axis.⁴ Recently, we demonstrated that this effect of polarization filtering can be dynamically reduced by additional optical pumping, if a linearly polarized pump beam bleaches the absorption by creating carriers in one of the two or both uppermost VBs.⁵

For the investigated GaN film, a maximum dynamic rotation of the polarization vector of 35° was observed,⁵ which is close to the maximum value of static rotation of 40° suggesting that the filtering is nearly switched off by the pump. In addition, we concluded that the filtering process and its manifestation by the dynamic and static rotation of the polarization vector are much more effective in M -plane GaN films than for other semiconductors with an in-plane polarization anisotropy such as ZnO, where a static rotation of only 12° was observed.^{6,7}

In this paper, we report on a detailed investigation of the dynamic behavior of this polarization filtering effect in M -plane GaN. After discussing the experimental details in Sec. II, we will investigate in Sec. III the origin of the fast component by polarization- and temperature-resolved experi-

ments. In Sec. IV, we separate the incoherent transients due to the hole redistribution between the two uppermost VBs from the coherent coupling artifact. This separation is essential for the application of a rate-equation model, which is applied in Sec. V to extract time constants for the redistribution of holes between the two uppermost VBs. Finally, we summarize the results and draw some conclusion in Sec. VI.

II. EXPERIMENT

The M -plane GaN film has been grown by rf plasma-assisted molecular-beam epitaxy on a γ -LiAlO₂(100) substrate.^{8,9} The thickness of the film is $0.7 \mu\text{m}$ as revealed by cross-sectional scanning electron microscopy. In order to investigate the dynamic behavior of the polarization filtering, we performed time-resolved transmittance spectroscopy using the degenerate pump-and-probe technique. The layout of the setup is shown in Fig. 1(a). Pulses of 200 ps duration are supplied by the second harmonic of a femtosecond Ti:sapphire laser. The laser is tuned to an energy just above the fundamental energy gap of GaN, where the difference of the absorption coefficients $\Delta\alpha(E) = \alpha_{\perp}(E) - \alpha_{\parallel}(E)$ becomes largest. For our sample, this condition occurs for room temperature at 3.44 eV (360 nm). The pump and probe are separated by a beam splitter, creating an intensity ratio of more than 20:1 in order to avoid any influence of the probe beam on the optical polarization properties.

In the experiment, an accurate polarization control of the pump and probe pulses is essential. Therefore, two Glan-Taylor polarizers are used in order to fix the linear polarization of both beams. By additionally using two $\lambda/2$ plates, the polarization angle of the pump and probe pulses can be independently selected. As depicted in Fig. 1(b), both the incident polarization angle for the probe ϕ_{probe} and the pump polarization angle ϕ_{pump} are defined with respect to the c axis. A microscope objective is used to tightly focus the

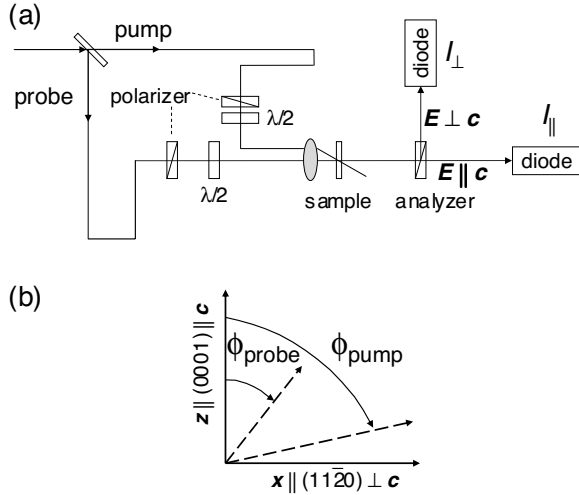


FIG. 1. (a) Layout of the pump-and-probe setup described in the text. (b) Definition of the polarization geometry with respect to the sample axes.

pump and probe beam onto the sample. The maximum achieved excitation density is about 5 mJ/cm². For low-temperature measurements, the sample is mounted in a standard helium flow cryostat. A second substrate is used to compensate the birefringence of the sample substrate. Depending on the experiment, either the transmitted probe signal is detected by a single photodiode connected to a lock-in amplifier or a Glan-Taylor analyzer is used to split the transmitted probe into its components $E \parallel c$ and $E \perp c$ and both are simultaneously detected by two photodiodes and two lock-in amplifiers.

III. FAST-TIME BEHAVIOR

The pump-induced changes in the absorption coefficient α can be quantified from the measured transmitted probe intensities $I_m(\tau)$, where $m = \perp$ and \parallel correspond to $E_{\text{probe}} \perp c$ and $E_{\text{probe}} \parallel c$, respectively, by the differential absorption coefficient

$$\Delta\alpha_m(\tau) = \frac{1}{d} \ln \left(\frac{I_m(\tau)}{I_{0,m}} \right), \quad (1)$$

where d denotes the film thickness, τ the delay time between the pump and probe pulses, and $I_{0,m}$ the transmitted probe intensity without the pump. Figure 2(a) shows $\Delta\alpha_m$ measured for $\phi_{\text{probe}} = 60^\circ$ and $E_{\text{pump}} \perp c$. First, if $E_{\text{pump}} \perp c$, the pump can only increase the occupation of the uppermost VB due to the polarization selection rules. Consequently, it is expected that only α_{\perp} will be modulated, which is in contradiction to the experimental result shown in Fig. 2(a), where α_{\parallel} is also clearly time dependent. Second, for $\Delta\alpha_{\perp}$ near $\tau = 0$, a fast component is visible with a time constant close to the resolution limit of the setup. This component also appears in $\Delta\alpha_{\parallel}$, if $E_{\text{pump}} \parallel c$ (not shown in Fig. 2), and is therefore directly correlated with the pump polarization. In Fig. 2(b), we show the ratio $\Delta\alpha_{\perp}/\Delta\alpha_{\parallel}$ in order to accurately determine the point in time where the fast decay is completed.

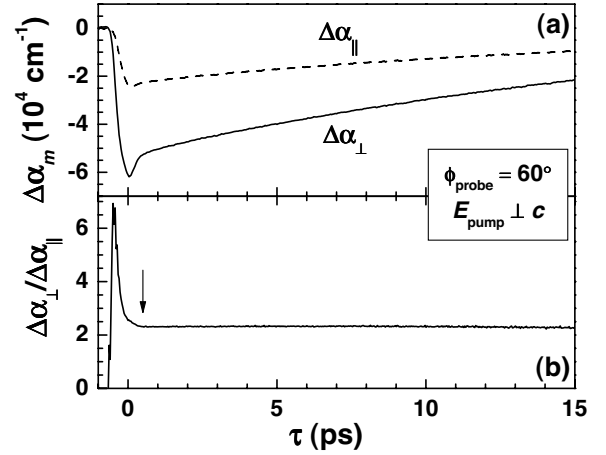


FIG. 2. (a) Pump-induced change of the absorption coefficients α_m as a function of the delay time τ for $\phi_{\text{probe}} = 60^\circ$ and $E_{\text{pump}} \perp c$ detected parallel (dashed line) and perpendicular to the c axis (solid line) at 300 K. (b) The ratio $\Delta\alpha_{\perp}/\Delta\alpha_{\parallel}$ as a function of τ . The arrow indicates the completion of the fast decay as described in the text.

The appearance of the fast component can be explained by the carrier redistribution between the two uppermost VBs or by the so-called coherent coupling artifact, which is well known in pump-and-probe experiments.¹⁰ In case of the redistribution, carriers move from the VB that is excited by the pump to the other VB and vice versa. We denote the transfer time of the holes between the two uppermost VBs by $\tau_{\perp \rightarrow \parallel}$ and $\tau_{\parallel \rightarrow \perp}$ and the occupation of the highest (second highest) VB by f_{\perp} (f_{\parallel}). The occupation f_m is related to the change in absorption by $\Delta\alpha_m = \alpha_m f_m$. The redistribution will take place until an equilibrium ratio of $f_{\perp}/f_{\parallel} \propto \tau_{\perp \rightarrow \parallel}/\tau_{\parallel \rightarrow \perp}$ is reached. After the redistribution is completed, the ratio $\Delta\alpha_{\perp}/\Delta\alpha_{\parallel} = \alpha_{\perp} f_{\perp}(t)/[\alpha_{\parallel} f_{\parallel}(t)]$ remains constant, in agreement with the experimental observation shown in Fig. 2(b). Note that the point in time for the completion of the redistribution, which is defined by the beginning of the constant part of the ratio in Fig. 2(b), coincides with the completion of the fast decay in Fig. 2(a) for the pumped VB, which suggests that the fast component is a result of the carrier transfer from the pumped VB to the unpumped one.

Since in our case the pump and probe pulses are derived from the same laser, one should take into account the coherent coupling artifact, which appears if both pulses overlap in time.^{11,12} The coherent part of the pump-and-probe signal corresponds to the third-order polarization radiating in the direction of the transmitted probe. This can be viewed as a diffraction of part of the pump pulse into the probe direction. We will now identify the coherent nature of the fast component in Fig. 2(a) in order to distinguish it from the fast decay due to the carrier redistribution.

Since the coherent part of the pump-and-probe signal is a function of the third-order polarization created by the pump and probe pulses in the GaN film, it should strongly depend on the polarization of both beams with respect to each other. The intensity of the pump that is diffracted into the probe direction should be maximized if pump and probe are polarized parallel to each other, while it should be minimized if they are cross polarized. The method of comparing the

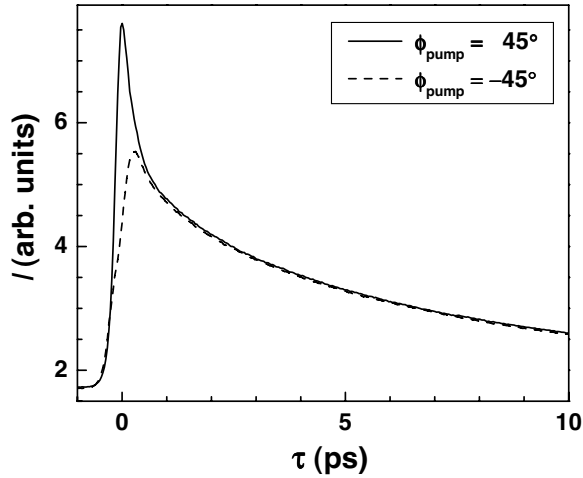


FIG. 3. Transmitted probe intensity I for $\phi_{\text{probe}}=45^\circ$ as a function of τ with $\mathbf{E}_{\text{pump}}\parallel\mathbf{E}_{\text{probe}}$ (solid line) and $\mathbf{E}_{\text{pump}}\perp\mathbf{E}_{\text{probe}}$ (dashed line) at 300 K.

pump-and-probe transients for these two configurations is often used to identify the coherent nature of such transients.¹⁰ As discussed above, the M -plane GaN film also shows carrier redistribution between the two uppermost VBs. Therefore, for such a comparison, two polarization configurations should be used, which create on the one hand the same starting point for the redistribution, but on the other hand can reduce or enhance the coherent artifact. In order to investigate the effect of these polarization configurations, we measure two pump-and-probe transients for $\phi_{\text{probe}}=45^\circ$ with either $\phi_{\text{pump}}=45^\circ$ ($\mathbf{E}_{\text{pump}}\parallel\mathbf{E}_{\text{probe}}$) or $\phi_{\text{pump}}=-45^\circ$ ($\mathbf{E}_{\text{pump}}\perp\mathbf{E}_{\text{probe}}$). Both angles of ϕ_{pump} will lead to the same initial ratio of the occupation factors f_{\perp}/f_{\parallel} so that the starting point for the redistribution will be the same, while the coherent artifact should be present only for $\mathbf{E}_{\text{pump}}\parallel\mathbf{E}_{\text{probe}}$. In Fig. 3, the experimental results for these two polarization configurations are shown. The fast component, which is strongly pronounced for $\mathbf{E}_{\text{pump}}\parallel\mathbf{E}_{\text{probe}}$ ($\phi_{\text{pump}}=45^\circ$), almost completely disappears for $\mathbf{E}_{\text{pump}}\perp\mathbf{E}_{\text{probe}}$ ($\phi_{\text{pump}}=-45^\circ$). This demonstrates the predominant coherent nature of the fast component. A careful inspection of the trace for $\phi_{\text{pump}}=-45^\circ$ shows that a small part of the fast component is still visible, which can be either due to an inaccuracy of the cross-polarized geometry of the pump and probe or due to carrier redistribution. We separately determined the polarization accuracy of the setup to be better than 5%.

For $\mathbf{E}_{\text{pump}}\perp\mathbf{E}_{\text{probe}}$, the influence of the carrier redistribution can be studied in more detail by varying ϕ_{probe} and ϕ_{pump} in such a way that $\phi_{\text{probe}}-\phi_{\text{pump}}=90^\circ$. We can distinguish two cases. For $\phi_{\text{probe}}=0^\circ$ and 90° , the projection of the pump polarization onto the state that is probed vanishes so that the carrier redistribution cannot create a fast component in the probe signal. However, for $\phi_{\text{probe}}\neq 0^\circ$ and 90° , the fast component can be created in the probe signal, which becomes largest for $\phi_{\text{probe}}=45^\circ$. In Fig. 4, we show the pump-and-probe transients for seven different values of ϕ_{probe} under the condition that $\mathbf{E}_{\text{pump}}\perp\mathbf{E}_{\text{probe}}$. A careful comparison of the traces for $\phi_{\text{probe}}=0^\circ$ and 90° with the traces for $\phi_{\text{probe}}=30^\circ, 45^\circ$, and 60° shows that the fast component that is

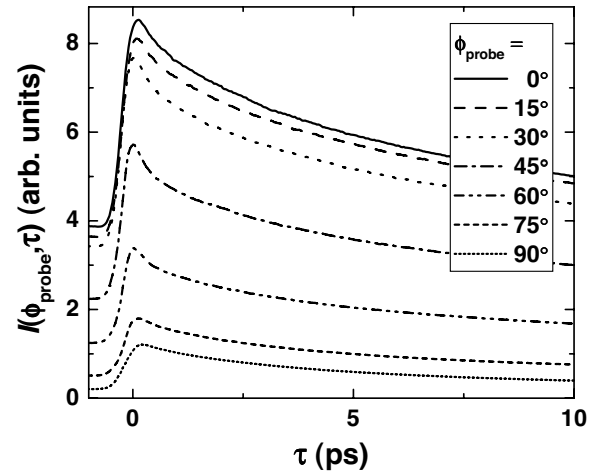


FIG. 4. Transmitted probe intensity I as a function of τ for various values of ϕ_{probe} keeping always $\mathbf{E}_{\text{pump}}\perp\mathbf{E}_{\text{probe}}$ ($\phi_{\text{probe}}-\phi_{\text{pump}}=90^\circ$) at 300 K.

present in the latter cases completely disappears in the former cases. The experimental results in Fig. 3 clearly demonstrate that the cross polarization of the pump and probe will remove the coherent artifact. Nevertheless, as shown in Fig. 4 for $\phi_{\text{probe}}\neq 0^\circ$ and 90° , the hole redistribution can still create a fast component on the time scale of the coherent artifact, but with a much lower amplitude.

Since the main intensity of the fast component is due to the coherent coupling artifact, we expect a strong dependence of the amplitude of the coherent artifact on the sample temperature. At low temperatures, scattering processes are generally reduced so that dephasing appears on a longer time scale. Since a long dephasing time will increase the third-order nonlinear polarization, it will enhance the amplitude of the fast component.^{12,13} In Fig. 5, we show the component of the transmitted probe perpendicular to the c axis for $\mathbf{E}_{\text{pump}}\perp c$ at four different temperatures a function of τ . Since

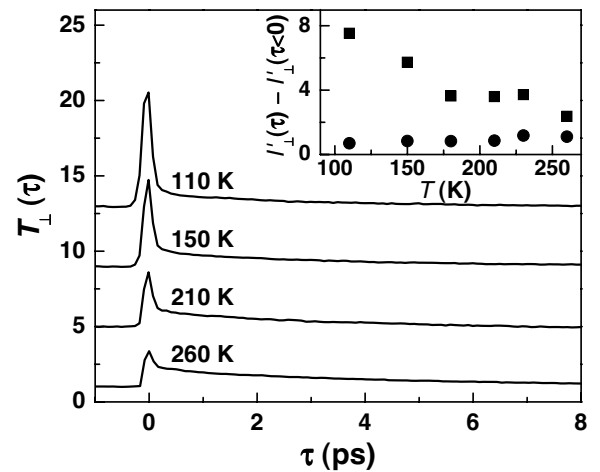


FIG. 5. Corrected transmitted probe intensity I'_{\perp} as a function of τ for $\phi_{\text{probe}}=60^\circ$ and $\mathbf{E}_{\text{pump}}\perp c$ recorded at different temperatures as indicated. Inset, pump-induced change in I'_{\perp} as a function of temperature T for overlapping pulses at $\tau=0$ ps (filled squares) and at $\tau=0.6$ ps (dots), where the fast decay is completed.

our sample exhibits a spatial inhomogeneity, we found slightly different ratios T_{\parallel}/T_{\perp} of the transmittances for different spot positions on the sample. In addition, due to the optical quality of the back side of the sample, the total transmission also varies with the spot position on the sample. We use a metal film on the sample surface with holes of 20 μm diameter in order to mark the positions where the experiments are performed. This is important because a variation of the temperature slightly changes the position of the sample with respect to the optical axis of the experiment. However, the diameter of the holes is still larger than the excitation spot so that additional corrections are necessary. Therefore, we plot in Fig. 5 the normalized intensity $I'_{\perp}(\tau) = I_{\perp}(\tau)/I_{\perp,\text{static}}$, where $I_{\perp}(\tau)$ denotes the measured intensity and $I_{\perp,\text{static}}$ the transmitted intensity without any pumping. Figure 5 clearly shows that if the temperature is reduced from 260 to 110 K the amplitude of the fast component is significantly enhanced. In the inset of Fig. 5, the pump-induced change of $I'_{\perp}(\tau)$ is shown for the maximum at $\tau=0$ (filled squares) and for $\tau=0.6$ ps (dots), where the fast decay is nearly completed. The inset of Fig. 5 demonstrates that the pump-induced change of $I'_{\perp}(\tau=0$ ps) becomes about three times larger if the temperature is reduced from 260 to 110 K, while the amplitude for the slow decay $I'_{\perp}(\tau=0.6$ ps) remains approximately the same. The observed temperature behavior clearly reveals the expected dependence discussed above. We conclude from both results, the polarization dependence and the temperature behavior, that the fast component is mainly due to the coherent coupling artifact.

IV. SEPARATION OF THE COHERENT ARTIFACT FROM THE HOLE REDISTRIBUTION

After demonstrating the origin of the fast component, it is necessary to extract more detailed information on the dynamic behavior of the redistribution between the two uppermost VBs from the pump-and-probe transients. For a detailed analysis of the dynamics, it is important to simultaneously measure $I_{\perp}(t)$ and $I_{\parallel}(t)$ by separate detectors exciting only one transition (e.g., $E_{\text{pump}} \perp c$) by the pump. Therefore, we use the original polarization configuration from Fig. 2. However, the transients in Fig. 2 are still masked by the coherent coupling artifact so that further data processing is indispensable in order to separate the coherent coupling artifact from the pump-induced changes in the absorption. For our sample, the dephasing time is expected to be very short, i.e., on the time scale of the length of the laser pulse, so that we can follow the approach of Heinz *et al.*¹⁴ and use the time symmetry property of the coherent coupling artifact to separate it from the incoherent change in the absorption. In our case, where the propagation directions of the pump and probe are almost collinear, the total signal in the probe direction can be divided in two parts,

$$I_m(\tau) = I^c(\tau) + I'_m(\tau), \quad (2)$$

where I^c denotes the intensity contribution of the coherent coupling artifact and I' denotes the one of the incoherent part of the transmitted probe. For the remainder of this paper, we

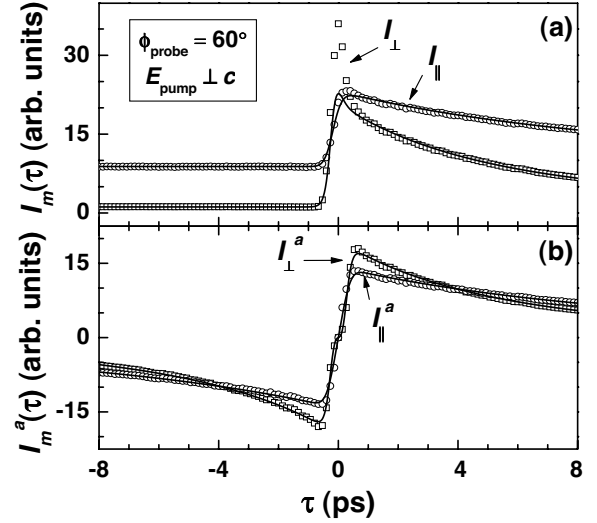


FIG. 6. (a) Transmitted probe intensity I_m as a function of τ detected parallel (circles) and perpendicular (squares) to the c axis. (b) Antisymmetric part of the transmitted probe intensity I_m^a as a function of τ as determined from the measured data (circles and squares) in (a) using Eq. (9). The solid lines in (a) and (b) indicate the fits to the model described in the text.

will assume that the pump and probe are collinear. In this case, the coherent part can be written as^{14,15}

$$I^c(\tau) \approx |\mathbf{e}_{\text{pump}} \cdot \mathbf{e}_{\text{probe}}|^2 \int \int_{-\infty}^{\infty} \text{Re}[E(t)E^*(t-\tau)]R^c(t-t') \times [E(t')E^*(t'-\tau)]dt't', \quad (3)$$

where \mathbf{e} denotes a unit vector in the direction of linear polarization of the corresponding beam, R^c the coherent response function of the system, and $E(t)$ the envelope function of the electric field, which is assumed to be the same for the pump and probe fields. The important point is that Eq. (3) can be shown to be symmetric with respect to the delay time τ , which yields $I^c(\tau) = I^c(-\tau)$. In contrast, the incoherent part $I'_m(\tau)$ does not contain a time-symmetric part. Therefore, looking at the antisymmetric part of the response

$$I_m^a(\tau) = \frac{1}{2}[I_m(\tau) - I_m(-\tau)] = \frac{1}{2}[I'_m(\tau) - I'_m(-\tau)], \quad (4)$$

the coherent artifact is completely removed, and we can use the antisymmetric part to extract the time constants for the redistribution. In Fig. 6(a), the measured transmitted probe intensities I_m (circles and squares) for an incident polarization angle of $\phi_{\text{probe}} = 60^\circ$ are shown, while in Fig. 6(b) the corresponding antisymmetric functions I_m^a are plotted.

V. RATE-EQUATION MODEL

In order to extract the characteristic time constants for the redistribution, we apply a two-level rate-equation model to describe the carrier transfer between the two uppermost VBs. Figure 7 summarizes the energy level structure together with the possible transitions, which were taken into account. Depending on ϕ_{pump} , the pump can create holes in the highest

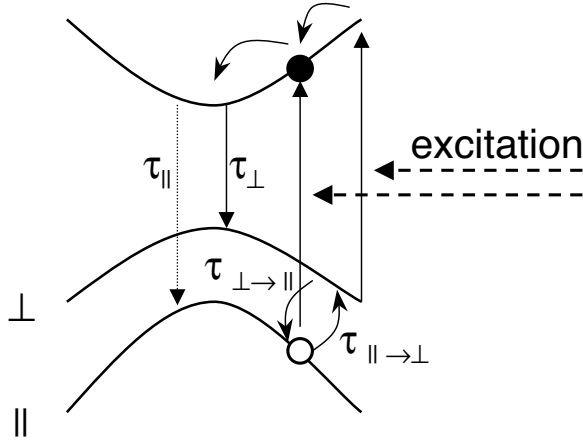


FIG. 7. Schematic diagram of the band structure introducing the decay times τ_{\perp} and τ_{\parallel} as well as the redistribution times $\tau_{\perp \rightarrow \parallel}$ and $\tau_{\parallel \rightarrow \perp}$ used in the rate equations of the hole redistribution model.

(\perp) and/or second highest (\parallel) VB by exciting the appropriate transition. Since we perform degenerate pump-and-probe experiments, both transitions can be only driven with the same energy so that these transitions will occur at slightly different \mathbf{k} values. After redistribution of the holes with the characteristic times $\tau_{\perp \rightarrow \parallel}$ and $\tau_{\parallel \rightarrow \perp}$ and further relaxation, the electron-hole pairs recombine near $\mathbf{k}=0$ with the recombination times τ_{\perp} and τ_{\parallel} . Under these conditions, the time derivative of the density of holes p_m in the two uppermost VBs is given by

$$\dot{p}_{\parallel} = G_{\parallel}(\tau, \hbar\omega, \phi_{\text{pump}})(1 - e^{-(1-f_{\parallel})\alpha_{\parallel}d}) - \frac{p_{\parallel}}{\tau_{\parallel}} + \frac{(1-f_{\parallel})p_{\perp}}{\tau_{\perp \rightarrow \parallel}} - \frac{(1-f_{\perp})p_{\parallel}}{\tau_{\parallel \rightarrow \perp}}, \quad (5)$$

$$\dot{p}_{\perp} = G_{\perp}(\tau, \hbar\omega, \phi_{\text{pump}})(1 - e^{-(1-f_{\perp})\alpha_{\perp}d}) - \frac{p_{\perp}}{\tau_{\perp}} - \frac{(1-f_{\perp})p_{\perp}}{\tau_{\perp \rightarrow \parallel}} + \frac{(1-f_{\perp})p_{\parallel}}{\tau_{\parallel \rightarrow \perp}}, \quad (6)$$

where G_m denotes the generation rate, $f_m = p_m/P_m$ the occupation numbers, and P_m the effective density of states in the VBs. Since the pump-induced change of the absorption coefficient is correlated with the occupation of the state and not with the carrier density, Eq. (5) can be rewritten in terms of the occupation numbers f_m resulting in

$$\dot{f}_{\parallel} = g_{\parallel}(\tau, \hbar\omega, \phi_{\text{pump}})(1 - e^{-(1-f_{\parallel})\alpha_{\parallel}d}) - \frac{f_{\parallel}}{\tau_{\parallel}} + \frac{(1-f_{\parallel})}{\beta} \frac{f_{\perp}}{\tau_{\perp \rightarrow \parallel}} - (1-f_{\perp}) \frac{f_{\parallel}}{\tau_{\parallel \rightarrow \perp}}, \quad (7)$$

$$\dot{f}_{\perp} = g_{\perp}(\tau, \hbar\omega, \phi_{\text{pump}})(1 - e^{-(1-f_{\perp})\alpha_{\perp}d}) - \frac{f_{\perp}}{\tau_{\perp}} - (1-f_{\parallel}) \frac{f_{\perp}}{\tau_{\perp \rightarrow \parallel}} + \beta(1-f_{\perp}) \frac{f_{\parallel}}{\tau_{\parallel \rightarrow \perp}}, \quad (8)$$

using $g_m = G_m/P_m$ and $\beta = P_{\parallel}/P_{\perp}$, the latter being of the same order of magnitude as $\alpha_{\parallel}/\alpha_{\perp}$.

The transmitted probe intensity is related to the occupation f_m by $I_{m,\text{calc}} = I_{0,m} \exp\{-[1 - f_m(\tau)]\alpha_m d\}$ so that the corresponding antisymmetric function is given by

$$I_{m,\text{calc}}^a(\tau) = \frac{I_{0,m}}{2} (\exp\{-[1 - f_m(\tau)]\alpha_m d\} - \exp\{-[1 - f_m(-\tau)]\alpha_m d\}). \quad (9)$$

The solid lines in Fig. 6(b) correspond to a fit of I_m^a using Eq. (9), where the system of Eqs. (7) and (8) is solved numerically. In addition, we used the constraint $I_{m,\text{calc}}(\tau < -1 \text{ ps}) = I_m(\tau = -1 \text{ ps})$ to reproduce the measured transients in Fig. 6(a). The fit yields values for the radiative lifetimes τ_m of about 15 ps, which are in agreement with the measured PL decay times. For the ratio of the effective density of states, we find a value of $\beta = 0.5$. This value is somewhat larger than the ratio of $\alpha_{\parallel}/\alpha_{\perp} = 0.23$ as independently determined in a cw-absorption experiment.¹⁶ For the redistribution times, we found $\tau_{\perp \rightarrow \parallel} = 0.44 \text{ ps}$ and $\tau_{\parallel \rightarrow \perp} = 0.23 \text{ ps}$. This indicates, that the hole redistribution between the two uppermost VBs is indeed very fast and efficient. It supports the observation of Omae *et al.*⁵ that the change of the absorption coefficients becomes nearly independent of the pump polarization after the fast decay is completed. Due to the efficient hole redistribution, which is much faster than the carrier recombination time, the ratio of f_{\perp}/f_{\parallel} is proportional to the ratio $\tau_{\perp \rightarrow \parallel}/\tau_{\parallel \rightarrow \perp}$. As expected, the determined ratio $\tau_{\perp \rightarrow \parallel}/\tau_{\parallel \rightarrow \perp} = 1.9$ is larger than one, because due to energy conservation the transition of carriers from the second highest VB to the highest VB becomes more probable than the transition in the opposite direction. This conclusion is supported by the temperature dependence of $\tau_{\perp \rightarrow \parallel}/\tau_{\parallel \rightarrow \perp}$, which increases by about a factor of 2 as compared to the room-temperature value with decreasing temperature down to 15 K. However, this ratio is not as large as expected, which is probably due to the high Fermi level originating from the large excitation density.

VI. SUMMARY AND CONCLUSIONS

We have investigated the origin of the fast component of optically induced absorption transients for an M -plane GaN film on $\gamma\text{-LiAlO}_2(100)$ at different temperatures. The fast component is dominated by the coherent coupling artifact. This is an important result for fast optical switching applications if the signal and the trigger are not coherent. Nevertheless, by separating the response into a symmetric (coherent artifact) and antisymmetric part (absorption bleaching), we determined the time constants of the hole redistribution between the two uppermost VBs by fitting the antisymmetric part to a rate-equation model. We observe a very efficient

redistribution of the holes between the two uppermost VBs. At the same time, we find that the occupations of both VBs only differ by about a factor of 2, after the redistribution is completed. Consequently, for device applications, a polarized signal beam can be switched by an unpolarized trigger beam since the hole redistribution is almost independent of the polarization direction of the pump. Finally, we conclude that *M*-plane GaN films exhibit polarization properties and

carrier redistribution times that make them promising candidates for ultrafast optical modulators with a high contrast.

ACKNOWLEDGMENTS

One of the authors (K.O.) acknowledges financial support from the Japan Society for the Promotion of Science.

*Electronic address: flissi@pdi-berlin.de

†Present address: Nitride Semiconductor Research Laboratory, Nichia Corporation, 491 Oka Kaminaka, Anan, Tokushima, 774-8601, Japan.

- ¹H. Shen, M. Wraback, J. Pamulapati, M. Dutta, P. G. Newman, A. Ballato, and Y. Lu, *Appl. Phys. Lett.* **62**, 2908 (1993).
- ²D. S. McCallum, X. R. Huang, A. L. Smirl, D. Sun, and E. Towe, *Appl. Phys. Lett.* **66**, 2885 (1995).
- ³S. Ghosh, P. Waltereit, O. Brandt, H. T. Grahn, and K. H. Ploog, *Phys. Rev. B* **65**, 075202 (2002).
- ⁴P. Misra, Y. J. Sun, O. Brandt, and H. T. Grahn, *Appl. Phys. Lett.* **83**, 4327 (2003).
- ⁵K. Omae, T. Flissikowski, P. Misra, O. Brandt, H. T. Grahn, K. Kojima, and Y. Kawakami, *Appl. Phys. Lett.* **86**, 191909 (2005).
- ⁶M. Wraback, H. Shen, J. Pamulapati, M. Dutta, P. G. Newman, M. Taysing-Lara, and Y. Lu, *Surf. Sci.* **305**, 238 (1994).
- ⁷M. Wraback, H. Shen, S. Liang, C. R. Gorla, and Y. Lu, *Appl. Phys. Lett.* **74**, 507 (1999).
- ⁸P. Waltereit, O. Brandt, M. Ramsteiner, R. Uecker, P. Reiche, and K. H. Ploog, *J. Cryst. Growth* **218**, 143 (2000).
- ⁹Y. J. Sun, O. Brandt, and K. H. Ploog, *J. Vac. Sci. Technol. B* **21**, 1350 (2003).
- ¹⁰A. von Jena and H. E. Lessing, *Appl. Phys.* **19**, 131 (1979).
- ¹¹E. P. Ippen and C. V. Shank, in *Ultrashort Light Pulses, Topics in Applied Physics*, edited by S. L. Shapiro (Springer, Berlin, 1977), Vol. 18.
- ¹²B. S. Wherrett, A. L. Smirl, and T. F. Boggess, *IEEE J. Quantum Electron.* **QE-19**, 680 (1983).
- ¹³M. W. Balk and G. R. Fleming, *J. Chem. Phys.* **83**, 4300 (1985).
- ¹⁴T. F. Heinz, S. L. Palfrey, and K. B. Eisenthal, *Opt. Lett.* **9**, 359 (1984).
- ¹⁵R. A. Engh, J. W. Petrich, and G. R. Fleming, *J. Phys. Chem.* **89**, 618 (1985).
- ¹⁶P. Misra, Y. J. Sun, O. Brandt, and H. T. Grahn, *J. Appl. Phys.* **96**, 7029 (2004).